A FRACTOGRAPHIC STUDY OF DAMAGE ACCUMULATION DURING FRACTURE OF TWO STEELS

K. AL-NABULSI[1] AND D.A. KOSS
Department of Materials Science and Engineering, Penn State University, University Park, PA 16802
[1]Currently MEU/ME&CCD Division, Saudi Aramco, P.O. Box 11660, Dhahran, Saudi Arabia 31311

ABSTRACT

While the two steels HY-100 and HSLA-100 have similar strengths and deformation behavior, the large inclusions in the HY-100 tend to be quite elongated and clustered in bands, while the HSLA-100 steel has nearly spherical inclusions that are more uniformly distributed. This study contrasts the damage accumulation that initiates at inclusions during ductile fracture of these two steels by examining the void area fractions present *on* the fracture surfaces of specimens pre-strained at room temperature and subsequently fractured in a brittle manner at -196^{0}C. The behavior of circumferentially notched specimens shows that a significantly larger void nucleation strain is the primary factor contributing to the higher ductility of the HSLA-100. Despite the differences in void shape and distribution of the two steels, the fracture surface results suggest that, once voids nucleate, the rate of damage accumulation with strain is surprising similar with significant void interaction effects accelerating damage accumulation in both steels.

1 INTRODUCTION

Tensile fracture of ductile alloys typically occurs by a damage accumulation process involving void nucleation, void growth, and void coalescence. Experimental studies describing the evolution of the damage accumulation as a function of strain have usually relied on a metallographic examination of *planar* cross sections of fractured tensile specimens. In this procedure, a failed round bar tensile specimen is sectioned along its length, and quantitative metallography is used to determine the local values of damage (area fractions and densities of voids) as a function of distance from the fracture surface of the (usually) necked tensile specimen. Measurement of the local strain also as a function of distance from the fracture surface then provides the basis for relating the observed damage accumulation to plastic strain.

The results from the planar cross section procedure are limited to reports of damage *beneath* the fracture surface and interpretation of such results requires an extrapolation to behavior on the fracture surface. In the present study, we examine damage evolution *on* the fracture surface by pre-straining circumferentially notched tensile specimens at room temperature to initiate ductile damage and subsequently fracturing the specimens in a brittle manner below their ductile to brittle transition temperature. This study is based on the two steels HY-100 and HSLA-100 previously examined for damage accumulation using the planar cross-section procedure [1,2]. Both steels have similar yield strengths and strain hardening characteristics, but the HSLA-100 shows significantly better tensile ductility over a range of stress triaxialities [1-4].

2 EXPERIMENTAL PROCEDURE

The materials examined in the current project were the same quenched and tempered HY-100 and HSLA-100 steel base-plates used in previous studies [1-4]. Both steels have low levels of inclusions (HY-100 has an inclusion volume fraction of approx. 0.00015, while that of HSLA-100 is somewhat higher, approx. 0.0005). Importantly, the HSLA-100 steel had been calcium treated

for sulfide-shape control such that the sulfides are nearly spherical, not elongated as is typical of most steels, such as HY-100; see Fig. 1. Furthermore, as observed in previous investigations [2], energy dispersive analysis (EDS) of the particles the HSLA inclusions indicates the presence of Cal and Al and have a complex "bulls-eye" cross-section microstructure [5,6]. Thus, while the HY-100 and HSLA-100 steels have similar yield strengths (in the 700 MPa range) and strain-hardening behavior, they differ considerably in their inclusion chemistries and microstructures.

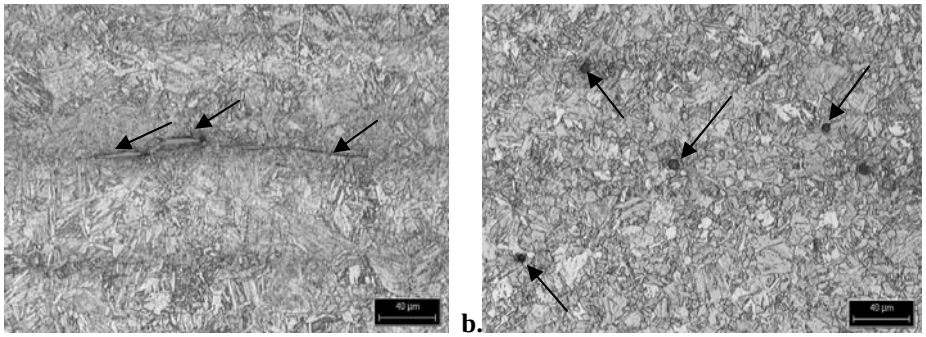

a. **b.**

Figure 1: A light micrograph showing (a) elongated inclusions present in HY-100 steel and (b) spherical inclusions (the dark phase) present in HSLA-100 steel. After ref's [1] and [2].

In order to localize damage, circumferentially notched round-bar tensile specimens (15.24 mm maximum diameter) were tested with an applied tensile loading axis corresponding to the long-transverse orientation of the plate. The radius of curvature of the circumferential notch (ρ) was 1.9 mm, while the minimum notch diameter was 2R = 7.6 mm; thus, $R/\rho = 2.0$ for this "D-notch" specimen geometry. For this geometry in both HY-100 and HSLA-100 steels, the stress triaxiality ratio $\sigma_m/\sigma_{eq} \approx 1.4$, where σ_m is the mean stress and σ_{eq} is the equivalent stress, assuming isotropic plasticity [1-4]. The plastic strain was measured using an extensometer placed across the minimum diameter of the specimen and extensional strain was determined from the following relationship: $\varepsilon_{ave.} = -2\ell n(d_1/d_0)$, where d_1 and d_0 are the instantaneous and initial diameters of the notch-root respectively. The tests were performed at a strain rate of $\approx 10^{-3}$/s [1-4]. The test procedure was one of the following: (a) strain to fracture at room temperature, (b) no strain at room temperature, but strained to brittle fracture at -196^{0}C, or (c) pre-strain at room temperature to selected fractions of the failure strain, interrupt the test and reduce load, cool to -196^{0}C in liquid nitrogen, and strain to fracture.

Previous experimental observations of "D-notch" tensile specimens show that for both HY-100 and HSLA-100, the damage accumulation concentrates and failure initiation occurs near the center ($\leq$ 1 mm) of these circumferentially notched specimens [1-3]. Consistent with these observations are finite element analyses that show the stress triaxiality ratio to be largest at radial distances $\leq$ 1 mm from the centermost element of the notch, decreasing significantly at larger radial distances [1,2]. Thus, we focused our fracture surface observations on the central 2 mm diameter region of these specimens, which corresponds to the central 7% of the initial cross section area.

In order to characterize ductile damage on the fracture surfaces of specimens pre-strained at room temperature and subsequently fractured at -196^{o}C, a composite digital image of the central 2mm region was created using scanning electron microscopy (SEM) at 80X. This magnification level provided sufficient resolution to detect the large primary voids ($\geq$ 5 μm) that control fracture in these two steels. Within a field of primarily cleavage fracture, the voids were identified and digitally outlined with an estimated resolution of ± 2 μm; regions in question were examined at

higher magnifications. Using a high pixel resolution (935 by 935 pixels) for the central 2 mm region, the projected area fraction of voids was determined by conducting a pixel count using Photoshop digital imaging software. In order to verify the accuracy of our digital technique, a manual procedure using point grid was also employed. Both techniques yielded similar values with the values obtained using the digital technique being 5-10% lower than those obtained using the point grid technique.

3 RESULTS AND DISCUSSION

Tensile specimens of both the HY-100 and the HSLA-100 steels were initially strained to fracture at room temperature in order to determine their fracture strains so that subsequent specimens could be pre-strained at different levels of the fracture strain. As shown in Figure 2 and consistent with earlier observations [1-4], the fracture surfaces of these two steels have distinctly different appearances for this long transverse direction of the plate. The fracture surface of the HY-100 has the characteristically layered appearance, Fig. 2a, as *elongated* voids grow and link by a void-sheet process, forming a fracture surface with a zig-zag profile [1,3,4]. Subsequent tests of this steel at -196^{0}C (i.e., brittle fracture) revealed the presence of very long MnS inclusions (identified by energy dispersive spectroscopy, EDS) that measure up to 450 μm long and 15 μm wide.

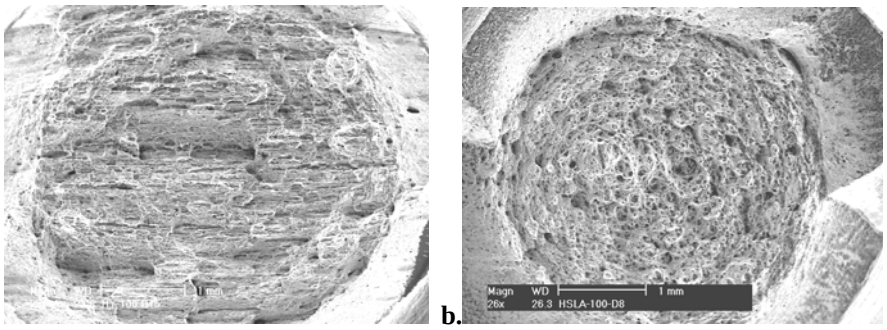

a. **b.**

Figure 2: Scanning electron micrographs showing the fracture surfaces of (a) HY-100 steel and (b) HSLA-100 steel specimens fractured at room temperature.

In contrast to HY-100, the HSLA-100 steel fails by the growth and coalescence to impingement of *equiaxed* voids, creating the fracture surface shown in Fig. 2b [2,4]. Consistent with Fig. 1b, the voids nucleate at spherical inclusions that range in size typically from 5 to 30 μm and are present as discrete particles and are relatively uniformly spaced. Occasionally, clusters of small particles residing in local bands that intersect the main fracture surface cause secondary cracks, which have only a minor effect on tensile ductility; specimens containing secondary cracking showed failure strains about ≈15% lower than those without.

Pre-straining the two steels at room temperature and subsequently fracturing them at -196^{0}C results in a fracture surface that is predominantly cleavage but with small regions of ductile damage, such as is shown in Fig's. 3a and 3c. For HY-100 steel with its elongated MnS inclusions, Fig 3a shows large, highly elongated voids, parallel to the surface of the plate and aligned in the rolling direction. A significant area fraction of voids are already present at small strains, ε_{ave} = 0.04, which is consistent with earlier observations based on planar sections normal to the fracture surface where well defined voids with considerable void growth are present at $\varepsilon < 0.05$ [1]. At higher levels of deformation, damage increase as large voids form from a combination of large fractured semi-continuous stringers of elongated MnS inclusions *and* a high density of small equiaxed MnS inclusions in the immediate vicinity of the stringers. Near material failure, very large flaws or "supervoids" form, typically are 600-1000 μm long and 60-100 μm wide and

oriented normal to the tensile axis. Material failure occurs as such flaws propagate under decreasing load conditions.

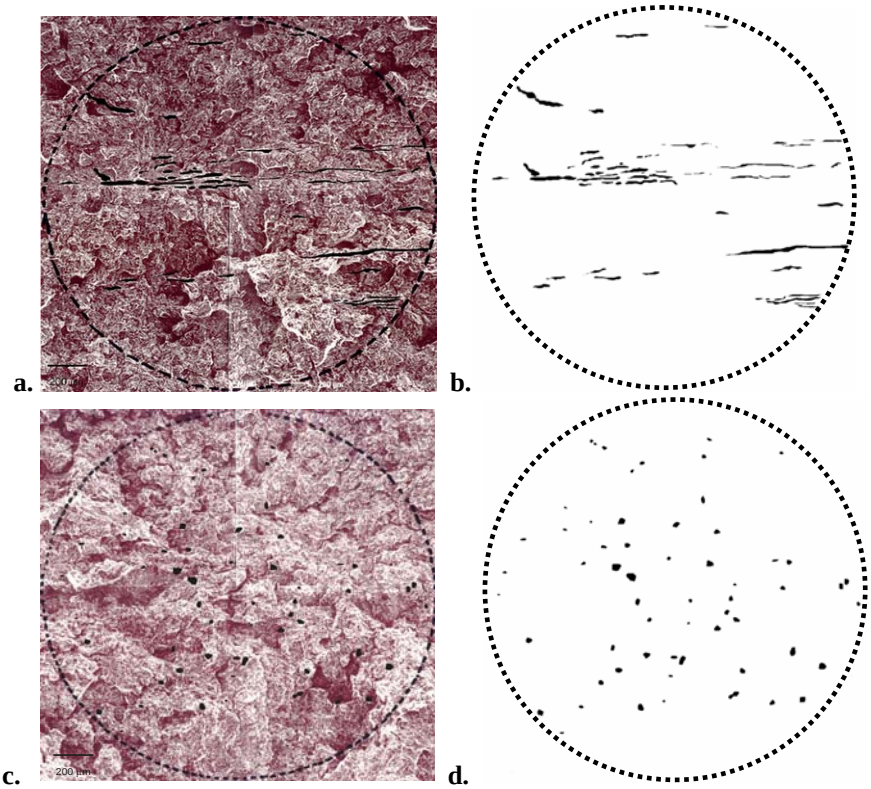

Figure 3: Fracture surfaces of (a) and (b) HY-100 steel pre-strained ($\varepsilon/\varepsilon_{fail} = 0.78$); (c) and (d) HSLA-100 steel pre-strained ($\varepsilon/\varepsilon_{fail} = 0.52$) at room temperature followed by fracture at -196^{0}C. Ductile damage is high-lighted.

In the HSLA-100 steel, no ductile voids were evident after a pre-strain of 0.06. Thus, a void nucleation strain $\varepsilon_{void} > 0.06$ (or greater than 30% of the failure strain) is necessary to initiate voids observable on the fracture surface. While it is possible that undetected voids did not coincide with subsequent brittle fracture surface, this apparent void nucleation strain is in fact similar to that reported ($\varepsilon_{void} \approx 0.06$) for HSLA-100 using the planar sectioning technique [2]. Thus, we conclude that finite void nucleation strain exists for the (Ca,Al)-modified inclusions even at this elevated level of stress triaxiality ($\sigma_m/\sigma_{eq} \approx 1.4$). At roughly 50% of the failure strain ($\varepsilon \cong 0.10$), ductile damage is quite evident, as seen in Fig. 3c, and it takes the form of small equiaxed voids that are well dispersed and form at spherical (Ca,Al)-modified inclusions.

After examining the fracture surface images such as Fig's. 3a and 3c, we have high-lighted the ductile damage to create the black-white contrasting images shown in Fig's. 3b and3d. This figure contrasts the damage evolution between these two steels not only in void shape but also in their spatial distribution. In the case of the HY-100 steel, Fig. 3b clearly shows that the elongated voids are quite *clustered* and tend to concentrate within elongated bands. As a result, ductile damage takes the form of long voids residing in neighboring parallel stringers, often spaced a projected distance of ≈50 μm apart, consistent with the microstrurctural banding in this steel [7].

In contrast to the HY-100, Fig's. 3c and 3d show damage in the HSLA-100 steel takes the form of equiaxed voids, which are more uniformly distributed throughout the matrix. The contrast in void shape and spatial distribution is quite apparent between the two steels; compare Fig's. 3b and 3d. At strain levels near fracture, void coalescence is beginning to occur in the HSLA-100, and the concentration of damage creates a few large voided areas.

Despite the differences in void shape and distribution, the number density of large "primary" voids ($\geq$ 5 μm) is similar between the two steels at strain levels $\varepsilon/\varepsilon_{failure} \geq 0.5$. Furthermore, there is only a small increase ($\leq$ 15%) in the density of the large voids in the range $0.5 \leq \varepsilon/\varepsilon_{failure} \leq 1.0$.

Based on the fracture surface observations, Fig. 4 shows the damage accumulation behavior of these two steels. Two behavior trends are apparent. First, as stated earlier and very evident in Fig. 4, while the HY steel appears to form voids at near zero strain, there is a significant void nucleation strain ($\varepsilon_{void} > 0.06$) in the HSLA-100. The result is a delay in the onset of ductile damage in the HSLA steel to larger strains, and this delay in forming voids appears to be the major factor in the increased ductility ($\Delta\varepsilon \cong 0.11$) of HSLA-100 when compared to the HY-100 steel.

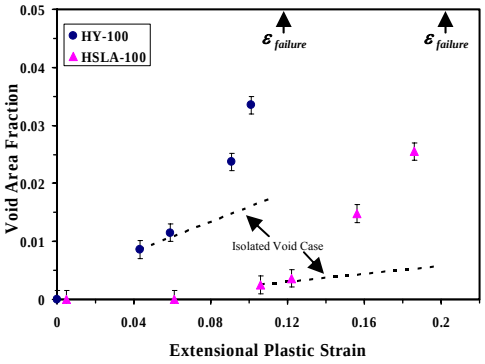

Figure 4: The dependence of the projected area fraction of voids as viewed on the fracture surfaces of HY-100 and HSLA-100 steels pre-strained and fractured at -196^{0}C.

The second trend evident in Fig. 4 is the similarity in the void growth behavior for the two steels. Despite differences in void shape and distribution, Fig. 3, the void growth rates are quite similar between the two steels once the voids nucleate as evident in Fig. 4. Comparison of the results in Fig. 4 with previous void growth behavior based on planar sections [1,2] shows similar behavior except that the absolute values of the area fraction of voids are factor of ≈10X higher in the present case. This difference is understandable in view of a ductile fracture path that links a high density of voids. For example, in the tensile failure of porous Ti, the fracture surface typically contains an area fraction of porosity that is a factor of ≈8X higher than bulk porosity [8].

Finally, we wish to comment briefly on the rate of void growth observed in Fig. 4 when compared to that predicted if the voids were isolated, non-interacting voids. For the case of HY-100, we approximate the elongated voids as holes growing according to the McClintock analysis [9], while for the HSLA-100, our reference basis is Rice and Tracey cavity-growth relationship for an isolated spherical void [10]. Both relationships describe the approximate radial growth of the cavities as follows:

$$\ln(R/R_o) \cong \alpha\varepsilon_{eq} \exp(\beta \frac{\sigma_m}{\sigma_{eq}}) \qquad (1)$$

where R_o and R are initial and final cavity radii, ε_{eq} is the equivalent far-field strain, α and β are constants whose values depend on void shape. For cylindrical hole-like cavities, $\alpha = 0.46$ and $\beta = 1.65$ for the strain hardening exponent ($n = d\ln\sigma/d\ln\varepsilon = 0.05$) of HY-100 [9]. For the near-spherical voids in HSLA-100, $\alpha = 0.427$ [11] and $\beta = 1.5$, according to Rice and Tracey [10].

Based on Eq. 1, Fig. 4 also shows the predicted void growth behavior over a strain increment during which there is little or no increase in the *density* of the large primary voids (> 5 μm). In both steels, the increase in damage as measured by void area fraction exceeds that predicted if the voids grew in an isolated manner. The significant increase of strain-induced damage accumulation most likely occurs due to void interaction effects that (a) accelerate void growth and (b) initiate void coalescence. The former might be expected for those voids spaced closely, such as those within one void diameter apart in Fig. 3.

4 CONCLUSIONS

The damage accumulation behavior of two steels (HY-100 and HSLA-100) with distinctly difference inclusion microstructures has been studied by pre-straining circumferentially notched tensile specimens at room temperature and subsequently fracturing the specimens at -196^0C. An examination of the ductile fracture regions of the fracture surfaces shows that, despite large differences in inclusion/void shape and distributions, the primary cause of the improved ductility of the HSLA-100 steel is a finite void nucleation strain. Once voids nucleate, the increase in the projected area fraction of voids with strain is quite similar for the two steels. In both cases, the rate of increase in void area exceeds that predicted by theory based on isolated voids, suggesting void interaction effects accelerate damage.

5 ACKNOWLEDGEMENTS

The authors are grateful to J. Bandstra and A. Glendening for discussions and assistance. The research was supported by Aramco Service Company. One of the authors (DAK) acknowledges the support of the Office of Naval Research.

6 REFERENCES

1. Jablokov, V., Goto, D.M., and Koss, D.A., Metall. and Mater. Trans.A, vol. 32A, 2985-2994, 2001.
2. Chae, D. and Koss, D.A., Mater. Sci. and Eng.A, vol. A366, 299-309, 2004.
3. Goto, D.M., Koss, D.A., and Jablokov, V., Metall. and Mater. Trans.A, vol. 30A, 2835-2842, 1999.
4. Goto, D.M., Chae, D., and Koss, D.A. in Mechanical Behavior of Materials (Fleming Printing Co., Victoria, BC), 150-155, 1999.
5. Wilson, A.D. in Inclusions and Their Influence on Material Behavior (ASM Int., Materials Park, OH), 21-34, 1988.
6. Kiessling, R. and Lang. N., Non-metallic Inclusions in Steels, 2nd Edition, (The Metals Society, London), 1978.
7. Chae, D., Koss, D.A., Wilson, A.L., andHowell, P.R., Metall and Mater. Trans.A., vol. 31A, 995-1005, 2000.
8. Bourcier, R.J. and Koss, D.A., Smelser, R.E., and Richmond, O., Acta Metall., vol. 34, 2443-2453, 1986.
9. McClintock, F.A., Ductility, (ASM, Metals Park, OH), 1968, p. 255.
10. Rice, J.R. and Tracey, D.M., J. Mech. Phys. Solids, vol. 17, 201-217, 1969
11. Huang, Y., J. Appl. Mech., vol. 29, 1509-1514, 1991.